# On the gradient calculation in 1.5-dimensional joint migration inversion

Sun, Y.; Verschuur, E.

**Publication date**
2021

**Document Version**
Final published version

**Published in**
82nd EAGE Conference and Exhibition 2021

**Citation (APA)**
Sun, Y., & Verschuur, E. (2021). On the gradient calculation in 1.5-dimensional joint migration inversion. In *82nd EAGE Conference and Exhibition 2021* (pp. 3398-3402). (82nd EAGE Conference and Exhibition 2021; Vol. 5). EAGE.

2021 EAGE ANNUAL
82ND CONFERENCE & EXHIBITION
AMSTERDAM | THE NETHERLANDS

# ON THE GRADIENT CALCULATION IN 1.5-DIMENSIONAL JOINT MIGRATION INVERSION

Y. Sun[1], E. Verschuur[2]

[1] Aramco Research Center - Delft; [2] Delft University of Technology

## Summary

The traditional joint migration inversion (JMI) technology faces the amplitude-versus-offset (AVO) challenge, which has been demonstrated before. We now apply JMI to 1.5-dimensional (1.5D) media, and use a velocity model and a density model to parameterize its solution space. As physically correct one-way propagation, reflection and transmission operators can be analytically formulated in 1.5D JMI, the AVO challenge is thus resolved. In this paper, we derive the complete theory behind the gradient calculation in 1.5D JMI, and further use a 1.5D synthetic example to demonstrate its correctness. This work is an important component of the 1.5D JMI theory, which will have applications in (locally) horizontally layered media containing strong multiple generators.

**On the gradient calculation in 1.5-dimensional joint migration inversion**

## Introduction

Joint migration inversion (JMI) is a recently proposed technology that explicitly uses multiples in seismic data for simultaneous velocity estimation and seismic migration (Berkhout, 2014b). JMI belongs to the school of full-waveform inversion, and it aims at minimizing the mismatch between simulated data and measurements. The inversion engine of JMI is gradient-based (Sun et al., 2019), and the modeling engine is based on one-way operators (Berkhout, 2014a; Sun et al., 2018a). Because of practical challenges, the state-of-the-art JMI adopts angle-independent operators (Sun et al., 2018b) in its implementation. As a consequence, the amplitude-versus-offset (AVO) effect in measured data cannot be corrected addressed by JMI (Sun et al., 2020).

One way to partially mitigate this AVO challenge faced by JMI is by using a different definition for the cost function (Qu et al., 2018), but the result quality is case dependent. We propose to apply JMI to 1.5-dimensional (1.5D) media, and use a velocity model and a density model to parameterize the solution space. In 1.5D JMI, the AVO challenge is thus correctly resolved because one-way propagation, reflection and transmission operators can be analytically defined in this situation. For 1.5D JMI, the gradient calculation is still the pillar of its inversion engine. In this paper, we formulate the complete theory behind the gradient calculation in 1.5D JMI, and further use a 1.5D synthetic example to demonstrate its correctness.

## Gradient calculation in 1.5D JMI

Due to space limitation, we cannot show the theory behind the modeling engine and the 'inverse propagation' concept in 1.5D JMI in this paper. This detailed theory can be found in Sun and Verschuur (2021). Moreover, below we only list key results while leaving out concrete derivations to save space.

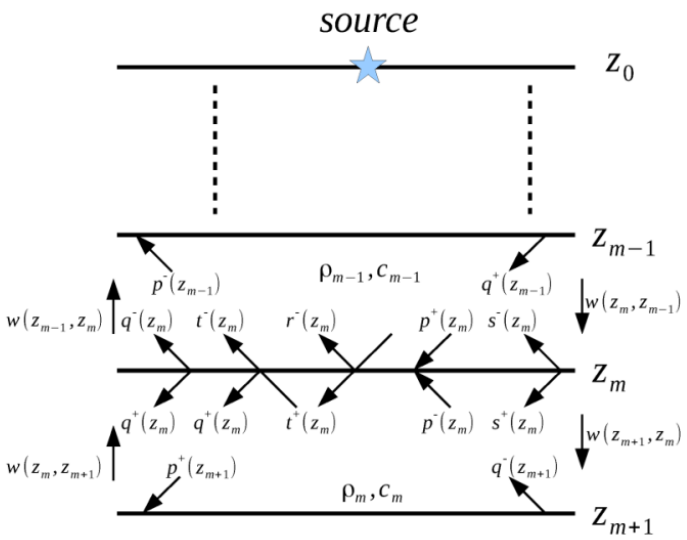


*Figure 1 The fundamental wavefield-propagation model in 1.5D JMI.*

Figure 1 shows the fundamental wavefield-propagation model in 1.5D JMI, where + or – represents the down-going or the up-going direction, $z_m$ is the depth of the m$^{th}$ interface in the z direction, $p$ is an incoming wavefield, $q$ is an outgoing wavefield, $t$ or $r$ is a transmission or reflection coefficient, $w$ is a one-way propagator, and $\rho_m$ and $c_m$ are medium density and velocity of the layer between $z = z_m$ and $z = z_{m+1}$. 1.5D JMI works in the temporal frequency – spatial wavenumber (FK) domain, so all the wavefield-related symbols on Figure 1 correspond to a certain combination of $k_x$ and $\omega$. For example, $q^+(z_m)$ there actually represents $q^+(z_m; k_x, \omega)$. The detailed mathematical definitions for all these symbols have been presented in Sun and Verschuur (2021).

Similar to the cost functions defined in the traditional JMI (Sun et al., 2019), we also define four cost functions at every subsurface depth level for 1.5D JMI using symbols mentioned above:

$$J_1(z_m) = \frac{1}{2}\left\|d_q^-(z_m) - q_n^-(z_m)\right\|^2, \quad (1)$$

$$J_2(z_m) = \frac{1}{2}\left\|d_q^+(z_m) - q_n^+(z_m)\right\|^2, \quad (2)$$

$$J_3(z_m) = \frac{1}{2}\left\|d_p^-(z_m) - p_n^-(z_m)\right\|^2, \quad (3)$$

$$J_4(z_m) = \frac{1}{2}\left\|d_p^+(z_m) - p_n^+(z_m)\right\|^2, \quad (4)$$

where $d_q^{\pm}(z_m)$ and $d_p^{\pm}(z_m)$ are our inversely propagated down-going (or up-going) outgoing (or incoming) wavefields from the measured surface wavefield $p_n^-(z_0)$, $q_n^{\pm}(z_m)$ and $p_n^{\pm}(z_m)$ are our simulated down-going (or up-going) outgoing (or incoming) wavefields. Note that all the symbols in equations (1) through (4) also correspond to a certain combination of $k_x$ and $\omega$. As mentioned above, different from the traditional JMI, we now treat medium parameters $\rho$ and $c$, rather than imaging parameters $t^{\pm}$, $r^{\pm}$ and $w$, as unknowns (Santosa and Symes, 1985) in 1.5D JMI.

Equations (1) through (4) are highly non-linear, and hence we have to adopt a linearization approximation: only one-way propagation, reflection and transmission operators $w$, $r^{\pm}$ and $t^{\pm}$ are functions of medium parameters $\rho$ and $c$, while wavefields $q_n^{\pm}(z_m)$ and $p_n^{\pm}(z_m)$ are not. Please note that $J_1(z_m)$ and $J_2(z_m)$ are functions of both $\rho$ and $c$ per definitions of $q_n^{\pm}(z_m)$, while $J_3(z_m)$ and $J_4(z_m)$ are functions of $c$ alone per definitions of $p_n^{\pm}(z_m)$ (Sun and Verschuur, 2021).

All gradients derived from equations (1) through (4) are shown as follows:

$$\frac{\partial J_1(z_m)}{\partial \rho_m} = Re\left\{\left[q_n^-(z_m) - d_q^-(z_m)\right]^* \cdot \frac{\partial q_n^-(z_m)}{\partial \rho_m}\right\}, \quad (5)$$

$$\frac{\partial q_n^-(z_m)}{\partial \rho_m} = \frac{-2\rho_{m+1}\cdot k_{z,m}\cdot k_{z,m+1}}{\left(\rho_{m+1}\cdot k_{z,m} + \rho_m \cdot k_{z,m+1}\right)^2} \cdot \left[p_n^+(z_m) - p_n^-(z_m)\right], \quad (6)$$

$$k_{z,m} = \begin{cases} \frac{\sqrt{\omega^2 - k_x^2 \cdot c_m^2}}{c_m}, & if \quad k_m^2 \geq k_x^2 \\ -i \cdot \frac{\sqrt{k_x^2 \cdot c_m^2 - \omega^2}}{c_m}, & otherwise \end{cases}, \quad (7)$$

$$\frac{\partial J_1(z_m)}{\partial c_m} = Re\left\{\left[q_n^-(z_m) - d_q^-(z_m)\right]^* \cdot \frac{\partial q_n^-(z_m)}{\partial c_m}\right\}, \quad (8)$$

$$\frac{\partial q_n^-(z_m)}{\partial c_m} = \frac{2\cdot\rho_{m+1}\cdot\rho_m\cdot k_{z,m+1}}{\left(\rho_{m+1}\cdot k_{z,m} + \rho_m \cdot k_{z,m+1}\right)^2} \cdot \left[p_n^+(z_m) - p_n^-(z_m)\right] \cdot \frac{\partial k_{z,m}}{\partial c_m}, \quad (9)$$

$$\frac{\partial k_{z,m}}{\partial c_m} = \begin{cases} -\frac{\omega^2}{c_m^2\sqrt{\omega^2 - k_x^2 \cdot c_m^2}}, & if \quad k_m^2 \geq k_x^2 \\ -i\frac{\omega^2}{c_m^2\sqrt{k_x^2 \cdot c_m^2 - \omega^2}}, & otherwise \end{cases}, \quad (10)$$

$$\frac{\partial J_2(z_m)}{\partial \rho_m} = Re\left\{\left[q_n^+(z_m) - d_q^+(z_m)\right]^* \cdot \frac{\partial q_n^+(z_m)}{\partial \rho_m}\right\}, \quad (11)$$

$$\frac{\partial q_n^+(z_m)}{\partial \rho_m} = \frac{-2\cdot k_{z,m+1}\cdot k_{z,m}\cdot \rho_{m+1}}{\left(\rho_{m+1}\cdot k_{z,m} + \rho_m \cdot k_{z,m+1}\right)^2} \cdot \left[p_n^+(z_m) - p_{n-1}^-(z_m)\right], \quad (12)$$

$$\frac{\partial J_2(z_m)}{\partial c_m} = Re\left\{\left[q_n^+(z_m) - d_q^+(z_m)\right]^* \cdot \frac{\partial q_n^+(z_m)}{\partial c_m}\right\}, \quad (13)$$

$$\frac{\partial q_n^+(z_m)}{\partial c_m} = \frac{2\cdot\rho_{m+1}\cdot\rho_m\cdot k_{z,m+1}}{\left(\rho_{m+1}\cdot k_{z,m} + \rho_m \cdot k_{z,m+1}\right)^2} \cdot \left[p_n^+(z_m) - p_{n-1}^-(z_m)\right] \cdot \frac{\partial k_{z,m}}{\partial c_m}, \quad (14)$$

$$\frac{\partial J_3(z_m)}{\partial c_{m+1}} = Re\left\{\left[q_n^-(z_{m+1})^* \cdot q_n^-(z_{m+1}) \cdot w(z_m, z_{m+1}) - d_p^-(z_m) \cdot q_n^-(z_{m+1})^*\right]^* \cdot \frac{\partial w(z_m, z_{m+1})}{\partial c_{m+1}}\right\}, \quad (15)$$

$$\frac{\partial w(z_m, z_{m+1})}{\partial c_{m+1}} = -i \cdot |z_{m+1} - z_m| \cdot \exp\left(-i \cdot k_{z,m+1} \cdot |z_{m+1} - z_m|\right) \cdot \frac{\partial k_{z,m+1}}{\partial c_{m+1}}, \quad (16)$$

$$\frac{\partial J_4(z_m)}{\partial c_m} = Re\left\{\left[w(z_m, z_{m-1}) \cdot q_n^+(z_{m-1}) \cdot q_n^+(z_{m-1})^* - d_p^+(z_m) \cdot q_n^+(z_{m-1})^*\right]^* \cdot \frac{\partial w(z_m, z_{m-1})}{\partial c_m}\right\}. \quad (17)$$

Note that equations (5) through (17) also correspond to a certain combination of $k_x$ and $\omega$. Following conventions used in the traditional JMI (Sun et al., 2019), we group contributions to the same medium parameter from different cost functions and different combinations of $k_x$ and $\omega$ together to formulate the final gradients for $\rho_m$ and $c_m$:

$$G(\rho_m) = \sum_\omega \sum_{k_x} [\frac{\partial J_1(z_m)}{\partial \rho_m} + \frac{\partial J_2(z_m)}{\partial \rho_m}] , \quad (18)$$

$$G(c_m) = \sum_\omega \sum_{k_x} [\frac{\partial J_1(z_m)}{\partial c_m} + \frac{\partial J_2(z_m)}{\partial c_m} + \frac{\partial J_3(z_m)}{\partial c_m} + \frac{\partial J_4(z_m)}{\partial c_m}] . \quad (19)$$

**Example**

We use a 1.5D synthetic model to demonstrate our derived gradients for 1.5D JMI. The correct amplitude spectrum of the source wavefield in our example is shown in Figure 2(a). As our purpose here is to demonstrate the correctness of our derived gradients, we take the true source wavefield as the a-priori information in our example. The true model is shown in Figure 2(b) in blue, and the data simulation plan is as follows: both the initial frequency and the frequency step are 0.2 Hz, and the maximum frequency is 30 Hz; the maximum source-receiver offset is 5 km, and the receiver spacing is 25 m; the grid size in the z direction is 5 m; we only consider internal multiples in this example, and we set the total iteration number to 10, meaning our surface wavefield contains primaries and 9 orders of internal multiples. We introduce a 1% perturbation to the thick layer between z=100 m and z=150 m to generate the wrong model for this example, as shown in Figure 2(b) in red. The surface receiver wavefields modeled using the true model and the wrong model are shown in Figures 2(c) and 2(d). When we use the true model as the input model for the gradient calculations, we expect gradients calculated by equations (18) and (19) to be 0s everywhere in our model space, and this is indeed the case shown in Figure 2(e). When we use the wrong model as the input model, equations (18) and (19) yield very clear gradients corresponding to the perturbed area in the true model, as shown in Figure 2(f).

**Conclusions**

In this paper, we formulate the complete theory for the gradient calculation in 1.5D JMI. Different from the traditional JMI, 1.5D JMI uses medium parameters as unknowns. We use a 1.5D synthetic example, with primaries and 9 orders of internal multiples accounted for, to demonstrate its correctness, and results are impressive. This work is an important component of the 1.5D JMI, and it paves a solid way to further develop the 1.5D JMI theory.

**References**

Berkhout, A. J., 2014a. Review Paper: An outlook on the future of seismic imaging, Part I: forward and reverse modelling: Geophysical Prospecting, 62, 911-930.

Berkhout, A. J., 2014b. Review Paper: An outlook on the future of seismic imaging, Part III: Joint Migration Inversion: Geophysical Prospecting, 62, 950-971.

Qu, S., Y. Sun and E. Verschuur, 2018. Mitigating amplitude versus ray-parameter effect in joint migration inversion using a zero-lag cross-correlation objective function of redatumed wavefields: SEG Technical Program Expanded Abstracts, 1133-1137.

Santosa, F. and W. W. Symes, 1985. The determination of a layered acoustic medium via multiple impedance profile inversion from plane wave responses: Geophysical Journal of the Royal Astronomical Society, 81, 175-195.

Sun, Y., E. Verschuur and R. van Borselen, 2018a. Acoustic propagation operators for pressure signals on an arbitrarily curved surface in a homogeneous medium: Journal of Applied Geophysics, 150, 314-324.

Sun, Y., E. Verschuur and S. Qu, 2019. Research note: Derivations of gradients in angle-independent joint migration inversion: Geophysical Prospecting, 67, 572-579.

Sun, Y., Y. S. Kim, Sh. Qu, E. Verschuur, A. Almomin and R. van Borselen, 2018b. Joint migration inversion versus FWI-RTM: a comparison study on a 2D realistic deep water model: EAGE Extended Abstract, Th P3 10.

Sun, Y., Y. S. Kim, S. Qu and E. Verschuur, 2020. Joint Migration Inversion: features and challenges: The Journal of Geophysics and Engineering, 17 (3), 525-538.

Sun, Y. and E. Verschuur, 2021. On the inverse propagation of receiver wavefields in 1.5-dimensional joint migration inversion: submitted to EAGE 2021.

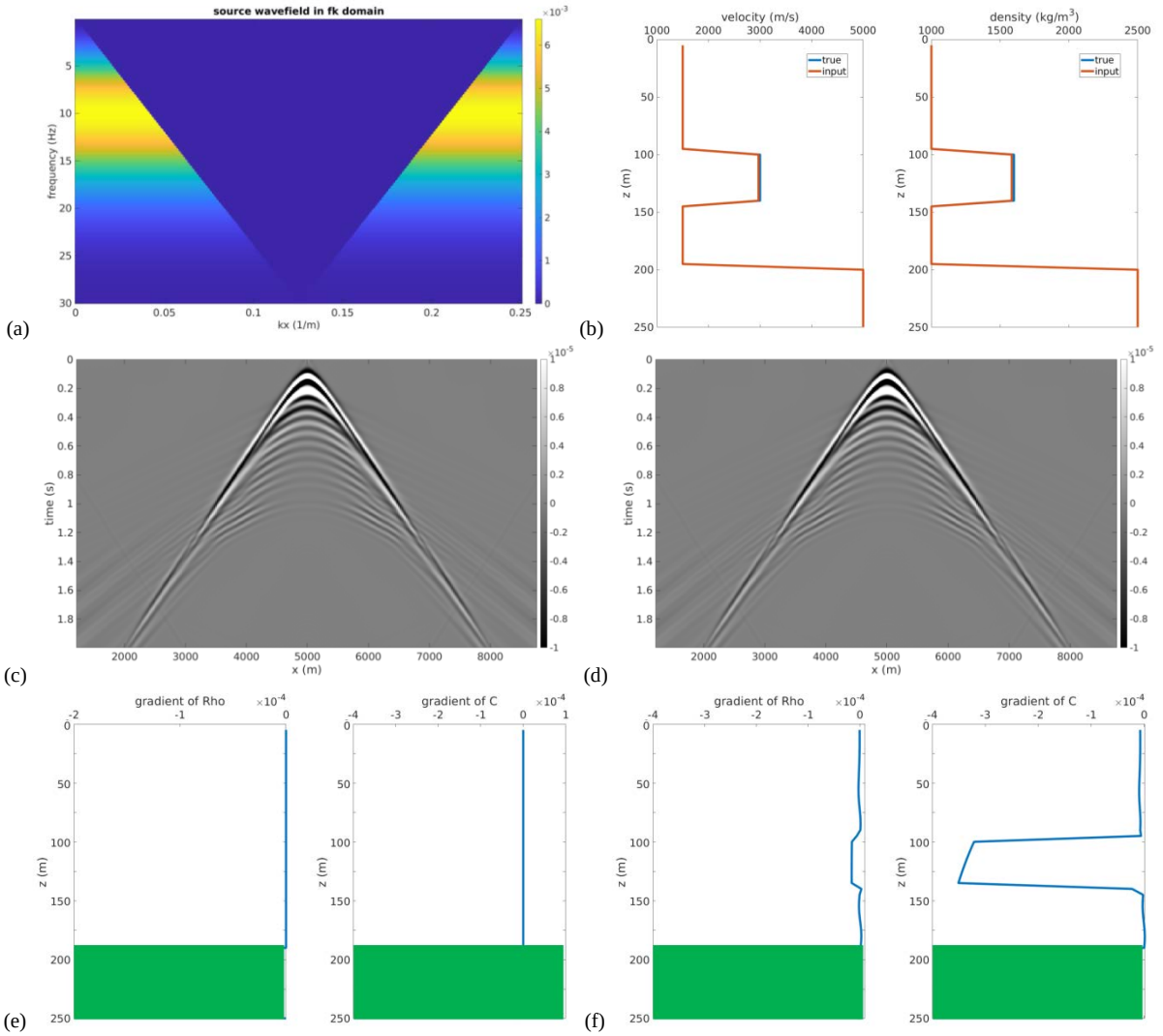


*Figure 2 (a) The amplitude spectrum of our source wavefield. (b) The true 1.5D model (blue) and a wrong model (red). (c) and (d) show the surface receiver wavefields from the true model and the wrong model shown in (b), including primaries and 9 orders of internal multiples. (e) and (f) show the gradients of the model when the input model is the true model or the wrong model shown in (b).*